Journal of Alloys and Compounds 703 (2017) 523–529

Contents lists available at ScienceDirect

Journal of Alloys and Compounds

journal homepage: http://www.elsevier.com/locate/jalcom

Effect of sodium chloride on the electrochemical corrosion of Inconel 625 at high temperature and pressure

Luying Wang [a, b], Heping Li [a, *], Qingyou Liu [a], Liping Xu [a], Sen Lin [a], Kai Zheng [a, b]

[a] Key Laboratory of High-temperature and High-pressure Study of the Earth's Interior, Institute of Geochemistry, Chinese Academy of Sciences, Guiyang, 550081, China
[b] University of Chinese Academy of Sciences, Beijing, 100039, China

ARTICLE INFO

Article history:
Received 28 September 2016
Received in revised form
24 January 2017
Accepted 29 January 2017
Available online 31 January 2017

Keywords:
Inconel 625
Sodium chloride
Oxide film
Polarization curves
EIS
SEM/EDS

ABSTRACT

The effect of sodium chloride (NaCl) on the electrochemical corrosion of the Inconel 625 at 300 ± 2 °C and 16 ± 1 MPa was investigated by polarization curves, electrochemical impedance spectroscopy (EIS) and scanning electron microscopy/energy dispersive X-ray spectroscopy (SEM/EDS). The experimental results showed that NaCl stimulated the Inconel 625 electrochemical corrosion and the oxide film on the surface of corroded Inconel 625 became less stable with increasing NaCl concentration. The oxide film was duplex with an inner Mg, Al-rich layer of $MgO+Al_2O_3$, with probably some Cr_2O_3, and an outer Ni-rich layer, principally $Ni(OH)_2/NiO$. The inner layer was more protective than the outer layer due to the precipitation of magnesium and aluminum oxide in the presence of Cl^-. In order to explain the corrosion behavior of the Inconel 625, an oxide film growth mechanism was discussed in this research.

© 2017 Elsevier B.V. All rights reserved.

1. Introduction

Ni-based alloys are often used in high temperature and high pressure aqueous environments. Though they are with high corrosion resistance, some corrosion problems are still observed, such as general corrosion, pitting corrosion, intergranular corrosion and stress corrosion cracking [1–7]. Inconel 625 is a high chromium, high molybdenum, nickel-based super alloy. The chromium contributes to enhance the corrosion resistance of Ni-based alloy and the molybdenum decreases the resistance of pitting corrosion [8–10]. At present, corrosion of Inconel 625 at high temperature and high pressure conditions has been widely investigated. An increase in temperature, pressure and dissolved oxygen could promote the corrosion process [11–13]. The oxide film on the surface of the corrosive material formed in these conditions was also researched by X-ray photoelectron spectroscopy (XPS) [14,15], scanning electron microscope/energy dispersive X-ray spectroscopy (SEM/EDS) [16,17], and X-ray powder diffraction (XRD) [18,19]. It was duplex-layer oxide structure, with nickel-rich oxides/hydroxides in the outer layer and chromium-rich oxides in the inner layer [14,20,21].

While Inconel 625 is widely used in harsh working conditions (high temperature and pressure) like paper industry, seawater heat changers and waste-fired boilers. chloride ions are the common ions in above condition [22]. Pitting corrosion and stress corrosion crack were observed in subcritical and supercritical water with chloride ions by surface analyses [23,24]. Therefore, chloride ion is a key factor to affect the corrosion of Inconel 625 in high temperature and high pressure solution. Though the corrosion of Inconel 625 is an electrochemical process, its electrochemical corrosion behavior was almost researched at low temperature and pressure, there were only a few in sub-critical and supercritical water environment [25,26]. As Sun et al. reported [11], it was attributed to three reasons: the first is the corrosion of the apparatus results in the change of solution; the second is the difficulty to develop an effective reference electrode to detect in situ electrochemical behavior at high temperature and pressure; the third is that controlling the electrochemical tests in high temperature and high pressure conditions is not easy. Solving these problems to investigate the effect of chloride ions on the corrosion of Inconel 625 in harsh working environment is necessary.

In this work, the electrochemical behavior of Inconel 625 in solution with different concentration of sodium chloride (NaCl) at

* Corresponding author.
E-mail address: hepingli123@yahoo.com (H. Li).

http://dx.doi.org/10.1016/j.jallcom.2017.01.320
0925-8388/© 2017 Elsevier B.V. All rights reserved.

300 ± 2 °C and 16 ± 1 MPa was investigated by polarization curves and electrochemical impedance spectroscopy (EIS) to reveal the passive mechanism of Inconel 625 under the influence of chloride ions. The oxide film on the surface of corroded Inconel 625 was examined by scanning electron microscopy (SEM) and energy-dispersive X-ray spectroscopy (EDS). Taking the conclusion of the electrochemical techniques and surface characterization measurements into consideration, the growth process of oxide film on the surface of Inconel 625 was discussed.

2. Experimental methods

2.1. Experimental facility and electrolyte preparation

All the experiments were performed in an autoclave with three electrodes, which was detailed described in another paper of our group [27]. The specimen is Inconel 625 from Beijing Chuanxianfeng Company. Its chemical composition is given in Table 1, in which the high concentration of carbon detected by EDS is due to the conductive adhesive contains carbon. The working electrode was prepared by cutting the Inconel 625 sample into a cone frustum with working areas of 0.148 cm^2. The auxiliary electrode was platinum auxiliary electrode, using conical alumina ceramic as the carrier and platinum powder was sintered on the two circular surfaces of the conical ceramic, with Pt wire insulating in the ceramic linking with the two surfaces. The area of exposed surface was 0.133 cm^2. The reference electrode was an Ag/AgCl pressure-balanced external reference electrode. Ag/AgCl wire was immersed into saturated KCl solution which worked as the reference electrode solution, therefore, all the potentials obtained in the following polarization curves correspond to the Ag/AgCl electrode in saturated KCl solution.

The experimental solutions were prepared by adding NaCl into ultrapure water, they were 0 mol/L, 0.025 mol/L, 0.05 mol/L, 0.1 mol/L and 0.2 mol/L, respectively. As the electrolyte was renewed before every experiment and the inside liner of the autoclave body was made of a titanium alloy Ti-3Al-2.5V, which is a highly corrosion resistance material, the electrolyte chemistry environmental was not significantly contaminated by its container.

2.2. Electrochemical measurements

Before each electrochemical measurement, the working electrode was successively abraded on 1500, 3000, 7000-grit silicon carbide papers, then rinsed with ultrapure water and acetone. While the temperature of electrolyte was raised up to 300 °C as Fig. 1, and the final temperature and corresponding pressure of the electrode were maintained at 300 ± 2 °C and 16 ± 1 MPa, respectively. Electrochemical measurements were performed using a computer-controlled electrochemical measurement system (PARSTAT 2263, Princeton Applied Research) with a conventional three-electrode electrolytic cell that included a platinum auxiliary electrode, an Inconel 625 working electrode and an Ag/AgCl pressure-balanced external reference electrode. The OCP of the cell were recorded for four hours in different NaCl concentration (0 mol/L, 0.025 mol/L, 0.05 mol/L, 0.1 mol/L and 0.2 mol/L) to reach a stable value after the autoclave started to be heated. Afterward, the EIS tests were performed at OCP and in the frequency range of 0.01–10.0000 HZ with a peak-to-peak amplitude of 10 mV and then the polarization curves were obtained by changing the electrode potential automatically from −0.4 to +1.3 V (vs. open current potential, OCP) at a scan rate of 2 mV s^{-1}. ZSimpWin 3.20 (2004) software was then used to fit the impedance data. To ensure reproducibility, identical experiments were repeated at least three times to ensure that the reported results were reproducible (i.e., the random errors of all three identical experimental results were within tolerance), and all of the reported results in this study were averaged.

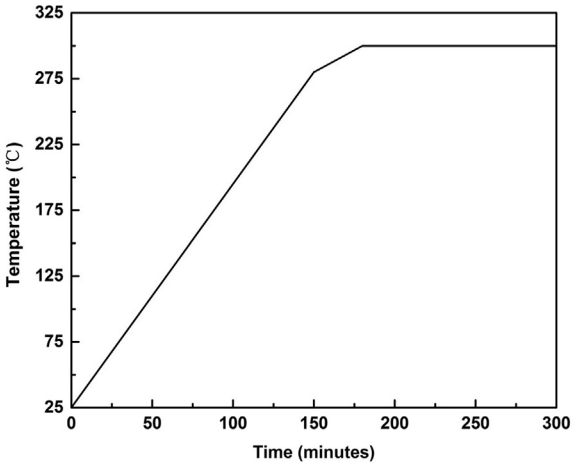

Fig. 1. Heating process of the autoclave.

2.3. Surface characterization measurements

After the Inconel 625 sample was abraded and cleaned, it was exposed to the solution with different concentration of NaCl (0 mol/L, 0.05 mol/L, 0.1 mol/L and 0.2 mol/L) at 300 ± 2 °C and 16 ± 1 MPa for 10 h. The surface morphologies of corroded samples were examined by the JSM-7800F scanning electron microscopy (SEM) and the chemical compositions of oxide films were investigated using the connected Apollo XL energy-dispersive X-ray spectroscopy (EDS).

3. Results and discussion

3.1. Polarization curves

Fig. 2 shows the polarization curves of the Inconel 625 electrode in the solution with different concentrations of NaCl (0 mol/L, 0.025 mol/L, 0.05 mol/L, 0.1 mol/L and 0.2 mol/L) at 300 ± 2 °C and 16 ± 1 MPa, with a scan rate of 2 mV s^{-1}. It was observed that the anodic current density was almost constant throughout the positive scan of polarization curves in the electrolyte without NaCl, which is due to the stable oxide films formed on the surface of the Inconel 625 working electrode. The stable oxide films are mostly duplex of an outer $Ni(OH)_2$/NiO layer and an inner Cr_2O_3 layer [11,20]. After oxidation of Ni and Cr at the anode by reaction (1) and (2), they were hydrolyzed to $Ni(OH)_2$ and $Cr(OH)_3$ by reaction (3) and (4), respectively. As $Ni(OH)_2$ can exist metastably in water at

Table 1
EDS elemental analysis of Alloy 625 before corrosion.

Element	Ni	Cr	Mo	Al	Mg	Fe	Si	Nb	Ti	C
Concn. (wt%)	61.40 ± 1.22	21.14 ± 0.43	5.83 ± 0.40	0.07 ± 0.05	0.08 ± 0.07	4.50 ± 0.23	0.02 ± 0.02	2.03 ± 0.22	0.49 ± 0.12	4.45 ± 0.65

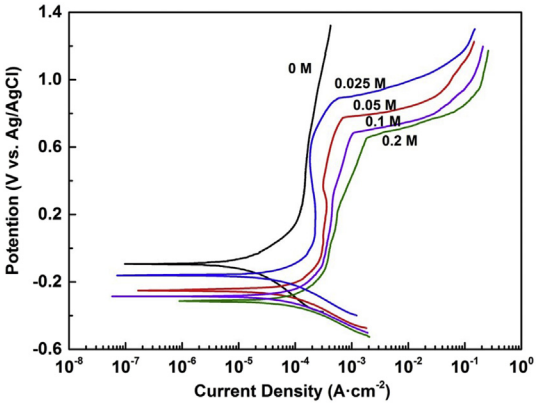

Fig. 2. The polarization curves of Inconel 625 in different C_{NaCl} solution at 300 ± 2 °C and 16 ± 1 MPa, with a scan rate of 0.166 mV/s.

temperatures on the order of 570 K for remarkably long periods and the presence of metastable $Ni(OH)_2$ results in the higher solubilities than $Ni(OH)_2$, the soluble $Ni(OH)_2$ was thermodynamically unstable with respect to NiO by reaction (5) [28–30]. In addition, the $Cr(OH)_3$ changed into Cr_2O_3 according to reaction (6) [11]. As the diffusivity of Cr in the oxide film was much smaller than that of Ni, the stable films was duplex of an inner Cr-rich layer and an outer Ni-rich layer [21].

$$Ni \rightarrow Ni^{2+} + 2e^- \quad (1)$$

$$Cr \rightarrow Cr^{3+} + 3e^- \quad (2)$$

$$Ni^{2+} + 2H_2O \leftrightarrow Ni(OH)_2 + 2H^+ \quad (3)$$

$$Cr^{3+} + 3H_2O \leftrightarrow Cr(OH)_3 + 3H^+ \quad (4)$$

$$Ni(OH)_{2(aq)} \leftrightarrow NiO_{(s)} + H_2O \quad (5)$$

$$Cr(OH)_3 + Cr \rightarrow Cr_2O_3 + 3H^+ + 3e^- \quad (6)$$

However, while the electrolyte contained NaCl, the unstable oxide films were examined. When starting the positive scan of polarization curves, though the passivation region was also observed, the anodic current density was slightly increased. It indicated the oxide film became less protective with increasing concentration of NaCl. Ni dissolution was strongest among dissolved metals of Inconel 625 at high temperature and pressure in the solution containing chloride ions [31,32]. The solubility of nickel oxide increased with increasing NaCl concentration [33]. Though chromium oxide solubility was the lowest among the three oxides (chromium, iron, and nickel), chromium oxide solubility increased when containing chloride ions in the solution [34].

When the potential increased, the anodic current density increased swiftly as the results of the decreasing oxide film at the transpassive region. Cr^{3+} was oxidized to hexavalent compound ($Cr_2O_7^{2-}$) in the transpassive state by reaction (7), which stimulated the dissolution of Cr_2O_3, leading to the breakdown of the oxide film [35]. In addition, the active potential of the Inconel 625 became more positive with increasing concentration of NaCl, which revealed the degraded corrosion resistance of the Inconel 625. Therefore, the chloride ions can effectively promote the Inconel 625 corrosion.

$$2Cr^{3+} + 7H_2O \rightarrow Cr_2O_7^{2-} + 14H^+ + 6e^- \quad (7)$$

Moreover, with the further positive scan of the potential, the passive tendency was observed at the end period of the polarization curves, which indicated that there was other oxide film formed on the surface of the Inconel 625. The chemical compositions of the oxide film were magnesium and aluminum oxides according to the following surface characteristics measurements of corroded Inconel 625. Al and Mg were oxidized to Al^{3+} and Mg^{2+} at the anode. Aluminum is precipitated as aluminum hydroxides at pH 5 [36]. As the pH of ultrapure water was 6.2, the aluminum precipitated as aluminum hydroxides and turned to aluminum oxide at high temperature. In addition, as Kravchenko et al. reported [37], magnesium oxidation takes place in aqueous solutions of alkali earth metals chlorides. Therefore, Al and Mg precipitated as Al_2O_3 and MgO. As Mg and Fe diffuse more slowly than Ni, the stable film was duplex of an inner Mg, Fe-rich layer and an outer Ni-rich layer. Being more compact of the inner layer led to the repassivation of the corroded Inconel 625.

We have calculated the electrochemical corrosion rate to further explained the effect of chloride ion on corrosion. The corrosion potential (E_{corr}), corrosion current density (i_{corr}; obtained using the Tafel extrapolation method), and passive current potential (i_{pass}) of Inconel 625 derived from polarization curves were exhibited as Table 2. With increasing NaCl concentration, the E_{corr} decreased from −0.088 ± 0.002 to −0.308 ± 0.003 V, the i_{corr} increased from 5.97 ± 0.27 to 25.48 ± 0.84 A cm^{-2} and the i_{pass} increased from 92.82 ± 5.09 to 371.92 ± 7.29 μA cm^{-2}, also confirming that the passive film became less stable. Therefore, NaCl could effectively stimulate the electrochemical corrosion of Inconel 625.

3.2. Electrochemical impedance spectroscopy

Fig. 3 presents the Nyquist plots of Inconel 625 in the electrolyte with different concentration of NaCl (0 mol/L, 0.025 mol/L, 0.05 mol/L, 0.1 mol/L and 0.2 mol/L) at 300 ± 2 °C and 16 ± 1 MPa. The Nyquist plots were composed of three depressed capacitive loops (Fig. 4). It is consistent with the surface structure of Inconel 625, on which the oxide film was composed of two layers. The first capacitive loop with high frequencies is attributed to the protective properties of the outer porous layer which is corresponding to the Ni-rich layer [20]. The second capacitive loop with middle frequencies is related to the passive properties of the inner porous layer. It is the Cr-rich layer in the solution without NaCl and the Mg, Al-rich layer in the solution with NaCl as the surface morphologies research of corroded Inconel 625. The third capacitive loop with low frequencies is attributed to the double layer between the Inconel 625 and the outer Helmholtz plane. As Zahrani et al. researched [38], the corresponding equivalent circuit model is shown in Fig. 4, where R_s is the electrolyte and other ohmic resistance, R_{osl} is the charge transfer resistance of ions through the outer porous layer, the constant phase element (CPE_p) is utilized to replace the capacitive behavior of outer porous layer due to frequency dispersion and surface inconsistencies and n shows the phase shift that can be explained as the degree of surface inhomogeneity, R_{isl} is the charge transfer resistance of ions through the inner porous layer, C_{isl} represents the corresponding capacitive

Table 2
Corrosion parameters associated with polarization of Inconel 625 electrodes.

C_{NaCl}/mol L^{-1}	E_{corr}/V	i_{corr}/μA cm^{-2}	i_{pass}/μA cm^{-2}
0	−0.088 ± 0.002	5.97 ± 0.27	92.82 ± 5.09
0.025	−0.163 ± 0.002	17.85 ± 0.88	106.32 ± 3.80
0.05	−0.258 ± 0.004	21.70 ± 0.84	173.79 ± 6.52
0.1	−0.286 ± 0.003	23.48 ± 0.66	256.90 ± 3.10
0.2	−0.308 ± 0.003	25.48 ± 0.84	371.92 ± 7.29

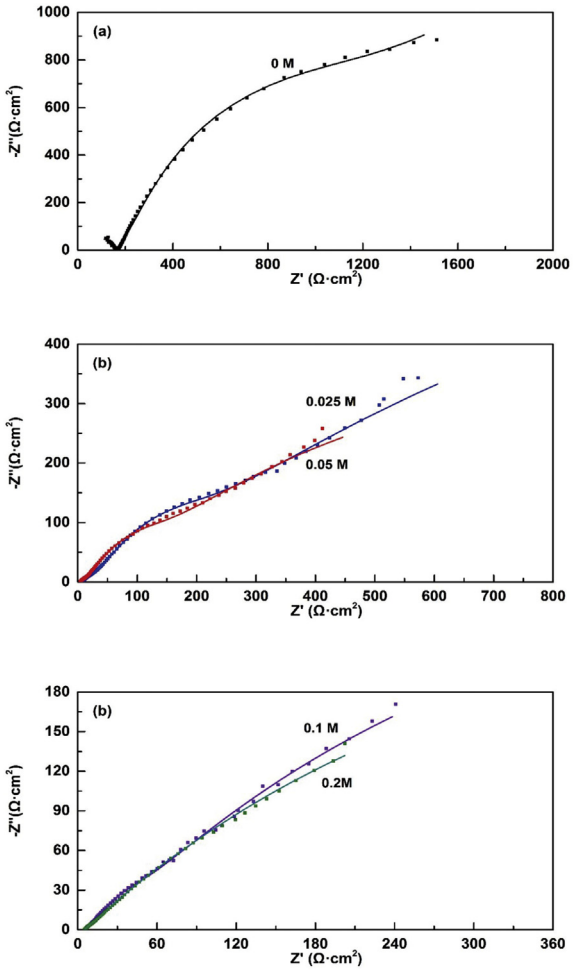

Fig. 3. Nyquist plots of Inconel 625 at OCP in different C_{NaCl} solution at 300 ± 2 °C and 16 ± 1 MPa.

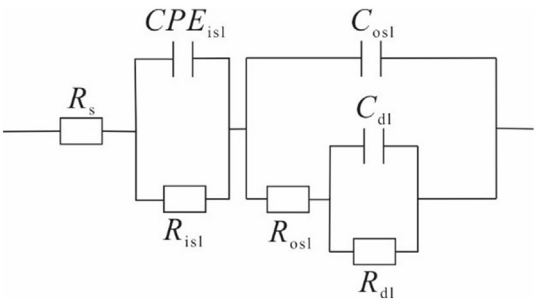

Fig. 4. Equivalent circuit of Inconel 625 in different C_{NaCl} solution at 300 ± 2 °C and 16 ± 1 MPa.

behavior of inner porous layer, R_{dl} and C_{dl} is the charge transfer resistance of ions through the double layer and the double layer capacitance, respectively.

The impedance parameters obtained by fitting the EIS data to the equivalent circuits are presented in Table 3. As the NaCl concentration increased, the values of R_{isl}, R_{osl}, R_{dl} were all decreased, which showed that chloride ions promoted the Inconel 625 corrosion. The conclusion of EIS was consistent with those from polarization curves study. A higher C_{dl} and lower R_{dl} indicated that the charges more easily diffused through the electric double layers, i.e., the electrochemical corrosion of Inconel 625 was easier. In addition, A lower R_{isl} and R_{osl} indicated that the passive film became less protective to inhibit Inconel 625 dissolution due to the strong penetration of chloride ions. While the R_{isl} value was much bigger than the R_{osl} value at the same NaCl concentration, the inner porous layer was the main passive factor. As nickel oxide were easier dissolved with increasing NaCl concentration and chloride ions could penetrate the passive film due to their small ionic radius, the R_{osl} value decreased dramatically [33]. Though the R_{isl} value also decreased, it decreased more smoothly with increasing NaCl concentration. NaCl can cause breakdown of protective oxide layers containing Cr_2O_3, which led to the decrease of the R_{isl} [39]. Meanwhile, Al and Mg precipitated by Al_2O_3 and MgO. Therefore, the concentration of Al_2O_3 and MgO at the inner layer increased with increasing NaCl concentration to form a new inner layer of the oxide film. The conclusion was accordance with the surface characteristics analyses of corroded Inconel 625.

3.3. Surface characterization measurements

The surface morphologies of corroded samples were investigated by scanning electron microscopy (SEM) and the element distribution of oxide films was determined using an energy-dispersive X-ray spectroscopy (EDS).

Fig. 5 shows the effects of chloride ions on the surface morphologies of the Inconel 625 after 10 h at 300 ± 2 °C and 16 ± 1 MPa. Before corrosion, the Inconel 625 sample was abraded and cleaned, there were no points of pitting corrosion (Fig. 5a). After exposing to the 0 mol/L NaCl solution for 10 h, pitting corrosion was observed on the surface of corroded Inconel 625 (Fig. 5b). As Tang et al. founded [40], the chloride and oxygen had the synergistic effect to alloy corrosion. While the concentration of NaCl solution was 0.2 mol/L, the points of pitting corrosion became more and bigger obviously (Fig. 5c). Therefore, the chloride ions effectively promoted Inconel 625 corrosion.

The X-ray mapping of Ni, Cr, O, Mg and Al about the oxide film of Inconel 625 in solution with different concentration of NaCl at 300 ± 2 °C and 16 ± 1 MPa were investigated (Fig. 6). The Ni and Cr concentration about the oxide film of pitting corrosion are lower than the surrounding, however, the O, Mg and Al concentration about the oxide film of pitting corrosion are higher than the surrounding. That's because Ni and Cr diffused into the solution by ions, while O, Mg and Al precipitated on the surface of Inconel 625 by the oxide. In addition, with the increasing chloride ions, we observed the deficiency of Ni and Cr and the gather of O, Mg and Al are more obvious. The oxidation mechanism of Inconel 625 in solution without/with NaCl at 300 ± 2 °C and 16 ± 1 MPa was exhibited in Fig. 7. As showed in Table 4, the Ni and Cr concentration decreased from 45.24 ± 0.90 wt% and 16.47 ± 0.33 wt% to

Table 3
Model parameters for equivalent circuit of Fig. 3

NaCl (mol L^{-1})	R_s (Ω cm^2)	CPE_{isl}, Y_0 (S cm^{-2} s^{-n})	n	R_{isl} (Ω cm^2)	C_{osl} (F cm^{-2})	R_{osl} (Ω cm^2)	C_{dl} (F cm^{-2})	R_{dl} (Ω cm^2)
0	68.830	4.091×10^{-3}	0.5555	9549	1.842×10^{-8}	696.90	5.702×10^{-3}	105.800
0.025	6.723	4.563×10^{-3}	0.4448	2932	2.663×10^{-4}	72.81	4.833×10^{-3}	4.747
0.05	3.922	6.236×10^{-3}	0.4817	1571	3.183×10^{-4}	51.30	6.690×10^{-3}	2.844
0.1	5.482	1.243×10^{-2}	0.5157	1113	1.846×10^{-3}	12.48	1.267×10^{-2}	1.788
0.2	1.298	1.320×10^{-2}	0.4814	1009	3.740×10^{-3}	2.682	2.362×10^{-2}	1.298

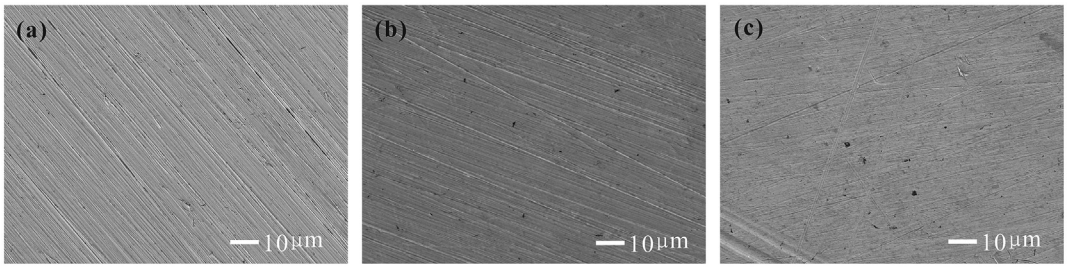

Fig. 5. SEM photomicrograph of Inconel 625 after 10 h exposure to different C_{NaCl} solution at 300 ± 2 °C and 16 ± 1 MPa: (a) before corrosion, (b) 0 mol/L and (c) 0.2 mol/L.

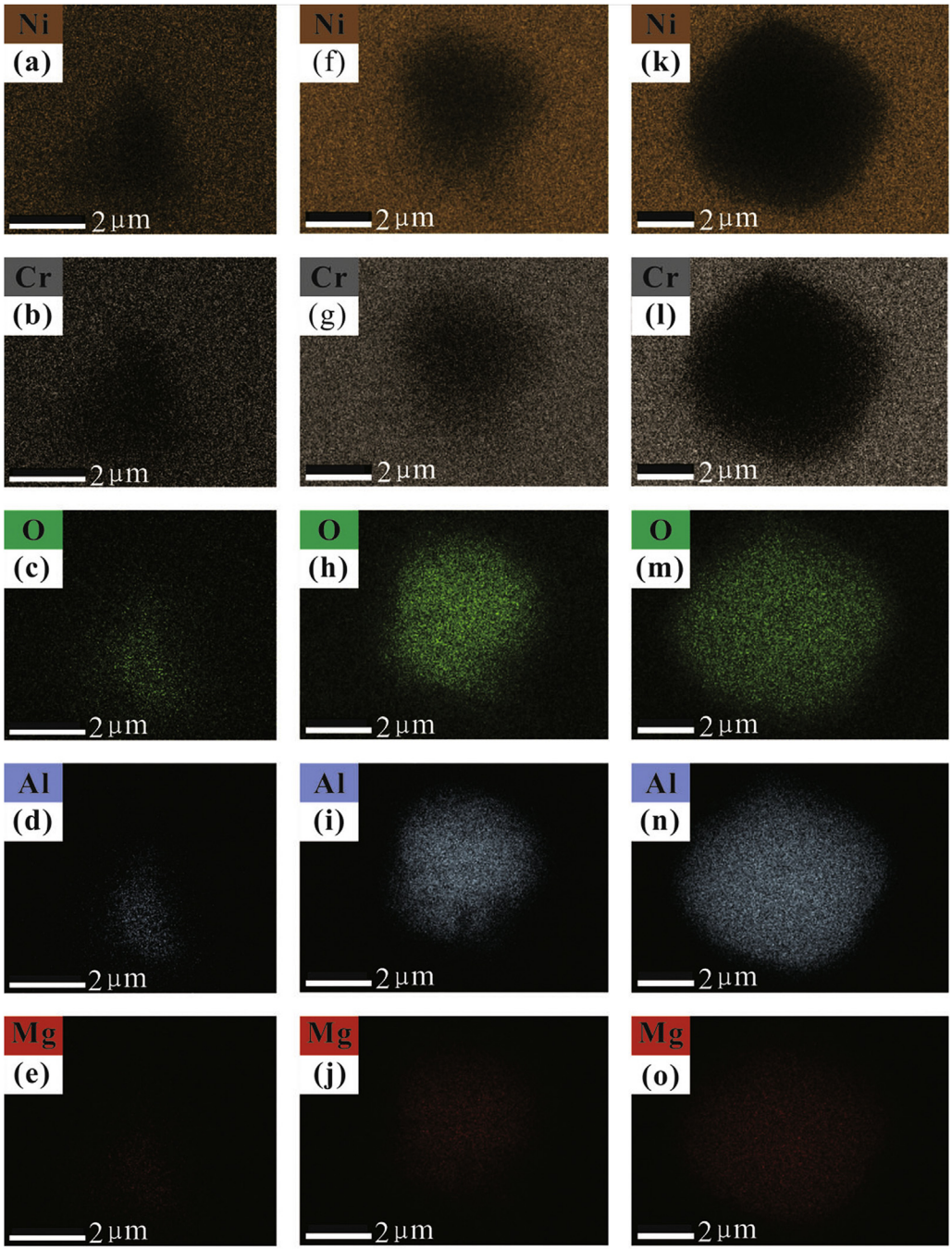

Fig. 6. EDS elemental analysis of Inconel 625 after 10 h exposure to different C_{NaCl} solution at 300 °C and 16 MPa: (a)(d) 0 mol/L; (b)(e) 0.05 mol/L and (c)(f) 0.2 mol/L.

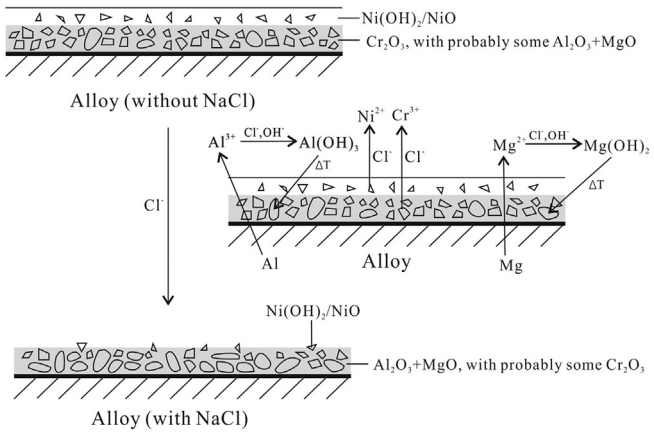

Fig. 7. The oxidation mechanism of Inconel 625 in solution without/with NaCl at 300 ± 2 °C and 16 ± 1 MPa.

10.29 ± 0.26 wt% and 5.00 ± 0.14 wt%, respectively, when the chloride ions increased from 0 mol/L to 0.2 mol/L. The significantly decreasing of Ni and Cr were due to the strong penetration of chloride through the oxide film and the increasing solubility of nickel and chromium oxide. Though Mo improves the pitting and crevice corrosion resistance of nickel-base alloys by forming a stable oxide in the dealloyed oxide layer, Mo itself without Cr does not provide suitable protection at high temperature and pressure [10,41]. As exhibited in Table 4, the Mo concentration decreased from 2.20 ± 0.23 wt% to 0.84 ± 0.11 wt%. It is in agreement with previous findings that the resistance of Mo degraded in the chemical composition of the penetrated molten phase [38]. However, comparing to the concentration of O, Mg and Al are 12.54 ± 1.14 wt%, 6.25 ± 0.61 wt% and 5.53 ± 0.63 wt% at 0 mol/L, they increase to 36.71 ± 3.04 wt%, 27.09 ± 1.93 wt% and 13.97 ± 1.06 wt% at 0.2 mol/L, respectively. There are two reasons. On the one hand, the concentration of Mg and Al grew on the surface of the alloy by the formation of magnesium and aluminum oxide; on the other hand, the deficiency of Ni and Cr further led to the increasing concentration of Mg and Al. The conclusion of oxide film analyses effectively explained the phenomenon of polarization curves and EIS.

4. Conclusions

The work investigated the influences of sodium chloride on the oxidizing dissolution of Inconel 625 at 300 ± 2 °C and 16 ± 1 MPa and further analyzed the oxide film grown on it, leading to the following conclusions:

Table 4
EDS elemental analysis (wt%) of Alloy 625 after 10 h exposure to different C_{NaCl} solution at 300 ± 2 °C and 16 ± 1 MPa.

	0 mol/L	0.05 mol/L	0.1 mol/L	0.2 mol/L
Ni	45.24 ± 0.90	26.98 ± 0.46	20.99 ± 0.36	10.29 ± 0.26
Cr	16.47 ± 0.33	11.10 ± 0.19	8.38 ± 0.17	5.00 ± 0.14
Mo	2.20 ± 0.23	1.45 ± 0.12	1.32 ± 0.12	0.84 ± 0.11
O	12.54 ± 1.14	24.92 ± 2.01	29.05 ± 2.43	36.71 ± 3.04
Al	6.25 ± 0.61	18.98 ± 1.51	20.80 ± 1.60	27.09 ± 1.93
Mg	5.53 ± 0.60	10.88 ± 0.88	12.85 ± 1.07	13.97 ± 1.06
Fe	4.40 ± 0.19	2.44 ± 0.10	0.62 ± 0.07	0.59 ± 0.09
Si	2.18 ± 0.22	0.18 ± 0.04	0.19 ± 0.04	0.27 ± 0.06
Nb	0.95 ± 0.14	0.46 ± 0.07	1.89 ± 0.13	1.81 ± 0.14
Ti	2.51 ± 0.11	1.24 ± 0.05	3.03 ± 0.09	1.77 ± 0.08
C	1.73 ± 0.33	1.38 ± 0.24	0.88 ± 0.19	1.67 ± 0.33

1. The oxide film on the surface of corroded Inconel 625 was consisted of two porous layers. The outer layer was Ni-rich layer and the inner layer turned from Cr-rich layer to Mg, Al-rich layer with increasing NaCl concentration due to the increasing solubility of Cr_2O_3.
2. NaCl stimulated the Inconel 625 electrochemical corrosion for two reasons: one is the strong penetration of chloride ions due to their small ionic radius; the other is the less stable oxide film grown on the surface of Inconel 625 due to the increasing dissolution of NiO and Cr_2O_3.
3. According to EIS results, the R_{isl} value was much bigger than the R_{osl} value at the same NaCl concentration, indicating the inner layer was more significant in inhibiting Inconel 625 dissolution comparing to the outer layer. While NiO of the outer layer dissolved by ions, Al and Mg precipitated by oxides to form the inner layer though Cr_2O_3 of the inner layer were also dissolved by ions in the presence of NaCl, resulting in that the outer layer was looser than the inner layer.

Acknowledgments

This work was financially supported by the National Key Research and Development Plan (2016YFC0600100), 135 Program of the Institute of Geochemistry, CAS, and Large-scale Scientific Apparatus Development Program (YZ200720), CAS.

References

[1] P. Kritzer, Corrosion in high-temperature and supercritical water and aqueous solutions: a review, J. Supercrit. Fluids 29 (2004) 1–29.
[2] X. Zhang, J. Hu, Y.Q. Wang, M.S. Zheng, Z.X. Zhang, Simulation of pitting corrosion for Ni-based alloy using a cellular automata model, Rare Metal. Mat. Eng. 44 (2015) 2347–2352.
[3] Z. Szklarskasmialowska, D. Grimes, J. Park, The kinetics of pit growth on alloy 600 in chloride solutions at high-temperatures, Corros. Sci. 27 (1987) 859–867.
[4] J.R. Park, Z. Szklarskasmialowska, Pitting corrosion of Inconel 600 in high-temperature water containing $CuCl_2$, Corrosion 41 (1985) 665–675.
[5] H.W. Cheng, B. Leng, K. Chen, Y.Y. Jia, J.S. Dong, Z.J. Li, X.T. Zhou, EPMA and TEM characterization of intergranular tellurium corrosion of Ni-16Mo-7Cr-4Fe superalloy, Corros. Sci. 97 (2015) 1–6.
[6] M. Payet, L. Marchetti, M. Tabarant, J.-P. Chevalier, Corrosion mechanism of a Ni-based alloy in supercritical water: impact of surface plastic deformation, Corros. Sci. 100 (2015) 47–56.
[7] H.R. Copson, G. Economy, Effect of some environmental conditions on stress corrosion behavior of Ni-Cr-Fe alloys in pressurized water, Corrosion 24 (1968), 55-&.
[8] N. Hara, S. Tanaka, K. Sugimoto, Corrosion behavior of constituent metals of stainless alloys in SCWO environments, in: Corrosion 2001, NACE International, 2001.
[9] N. Hara, S. Tanaka, S. Soma, K. Sugimoto, Corrosion resistance of Fe-Cr and Ni-Cr alloys in oxidizing supercritical HCl solution, in: Corrosion 2002, NACE International, 2002.
[10] H. Kim, D.B. Mitton, R.M. Latanision, Corrosion behavior of Ni-base alloys in aqueous HCl solution of pH 2 at high temperature and pressure, Corros. Sci. 52 (2010) 801–809.
[11] H. Sun, X. Wu, E.H. Han, Effects of temperature on the protective property, structure and composition of the oxide film on Alloy 625, Corros. Sci. 51 (2009) 2565–2572.
[12] T. Fujii, K. Sue, S.I. Kawasaki, Effect of pressure on corrosion of Inconel 625 in supercritical water up to 100 MPa with acids or oxygen, J. Supercrit. Fluids 95 (2014) 285–291.
[13] K.H. Chang, S.-M. Chen, T.K. Yeh, J.J. Kai, Effect of dissolved oxygen content on the oxide structure of Alloy 625 in supercritical water environments at 700°C, Corros. Sci. 81 (2014) 21–26.
[14] A. Machet, A. Galtayries, S. Zanna, L. Klein, V. Maurice, P. Jolivet, M. Foucault, P. Combrade, P. Scott, P. Marcus, XPS and STM study of the growth and structure of passive films in high temperature water on a nickel-base alloy, Electrochim. Acta 49 (2004) 3957–3964.
[15] M.S. Bakare, K.T. Voisey, M.J. Roe, D.G. McCartney, X-ray photoelectron spectroscopy study of the passive films formed on thermally sprayed and wrought Inconel 625, Appl. Surf. Sci. 257 (2010) 786–794.
[16] X. Xing, X. Di, B. Wang, The effect of post-weld heat treatment temperature on the microstructure of Inconel 625 deposited metal, J. Alloys Compd. 593 (2014) 110–116.
[17] N. Papageorgiou, A.V. Bonin, N. Espallargas, Tribocorrosion mechanisms of

NiCrMo-625 alloy: an electrochemical modeling approach, Tribol. Int. 73 (2014) 177–186.
[18] T.E. Abioye, D.G. McCartney, A.T. Clare, Laser cladding of Inconel 625 wire for corrosion protection, J. Mater. Process. Technol. 217 (2015) 232–240.
[19] Ö. Özgün, H.Ö. Gülsoy, R. Yilmaz, F. Findik, Injection molding of nickel based 625 superalloy: sintering, heat treatment, microstructure and mechanical properties, J. Alloys Compd. 546 (2013) 192–207.
[20] M. Sun, X. Wu, Z. Zhang, E.H. Han, Analyses of oxide films grown on Alloy 625 in oxidizing supercritical water, J. Supercrit. Fluids 47 (2008) 309–317.
[21] X. Zhong, E.H. Han, X. Wu, Corrosion behavior of Alloy 690 in aerated supercritical water, Corros. Sci. 66 (2013) 369–379.
[22] E. Mohammadi Zahrani, A.M. Alfantazi, Molten salt induced corrosion of Inconel 625 superalloy in $PbSO_4$–Pb_3O_4–$PbCl_2$–Fe_2O_3–ZnO environment, Corros. Sci. 65 (2012) 340–359.
[23] P. Kritzer, N. Boukis, E. Dinjus, Corrosion of alloy 625 in aqueous solutions containing chloride and oxygen, Corrosion 54 (1998) 824–834.
[24] H. Kim, D.B. Mitton, R.M. Latanision, Stress corrosion cracking of Alloy 625 in pH 2 aqueous solution at high temperature and pressure, Corrosion 67 (2011) 8.
[25] T. Zhang, H.Y. Jing, Y.D. Han, L.Y. Xu, Electrochemical behavior of corrosion resistance alloys, in: X.H. Liu, Z. Jiang, J.T. Han (Eds.), Materials Processing Technology, Pts 1-3, Trans Tech Publications Ltd, Stafa-Zurich, 2012, pp. 1097–1101.
[26] Z.F. Yin, W.Z. Zhao, W.Y. Lai, X.H. Zhao, Electrochemical behaviour of Ni-base alloys exposed under oil/gas field environments, Corros. Sci. 51 (2009) 1702–1706.
[27] S. Lin, H.P. Li, L.P. Xu, Y.Q. Zhang, C. Cui, Experimental set-up for three-electrode electrochemical measurement in high temperature and pressure fluids up to 700°C/1000 bar, (unpublished article).
[28] T.W. Swaddle, T.C.T. Wong, Hydrothermal reaction kinetics. The decomposition of nickel(II) hydrox, Can. J. Chem. 56 (2011) 363–369.
[29] P.R. Tremaine, J.C. Leblanc, The solubility of nickel-oxide and hydrolysis of Ni^{2+} in water to 573K, J. Chem. Thermodyn. 12 (1980) 521–538.
[30] S.E. Ziemniak, M.A. Goyette, Nickel(II) oxide solubility and phase stability in high temperature aqueous solutions, J. Solut. Chem. 33 (2004) 1135–1159.
[31] V. Kolarik, M. Wagner, B. Michelfelder, Corrosion of Alloys 625 and pure chromium in Cl-containing fluids during supercritical water oxidation (SCWO), in: Corrosion 99, NACE International, 1999.
[32] X.Y. Tang, S.Z. Wang, D.H. Xu, Y.M. Gong, J. Zhang, Y.Z. Wang, Corrosion behavior of Ni-based alloys in supercritical water containing high concentrations of salt and oxygen, Ind. Eng. Chem. Res. 52 (2013) 18241–18250.
[33] K. Sue, K. Arai, Calculation of solubility for metal oxide in supercritical water environments, Zairyo-to-Kankyo 53 (2004) 264–269.
[34] T. Adschiri, Y. Watanabe, K. Sue, K. Arai, Estimation of metal oxide solubility and understanding corrosion in supercritical water, in: Corrosion 2001, NACE International, 2001.
[35] D. Devilliers, M.T.D. Thi, E. Mahé, Q.L. Xuan, Cr(III) oxidation with lead dioxide-based anodes, Electrochim. Acta 48 (2003) 4301–4309.
[36] R.B. Martin, Fe^{3+} and Al^{3+} hydrolysis equilibria. Cooperativity in Al^{3+} hydrolysis reactions, J. Inorg. Biochem. 44 (1991) 141–147.
[37] O.V. Kravchenko, L.G. Sevastyanova, S.A. Urvanov, B.M. Bulychev, Formation of hydrogen from oxidation of Mg, Mg alloys and mixture with Ni, Co, Cu and Fe in aqueous salt solutions, Int. J. Hydrogen Energy 39 (2014) 5522–5527.
[38] E. Mohammadi Zahrani, A.M. Alfantazi, High temperature corrosion and electrochemical behavior of INCONEL 625 weld overlay in $PbSO_4$–Pb_3O_4–$PbCl_2$–CdO–ZnO molten salt medium, Corros. Sci. 85 (2014) 60–76.
[39] M.K. Hossain, S.R.J. Saunders, A microstructural study of the influence of NaCl vapor on the oxidation of a Ni-Cr-Al alloy at 850°C, Oxid. Met. 12 (1978) 1–22.
[40] X. Tang, S. Wang, L. Qian, Y. Li, Z. Lin, D. Xu, Y. Zhang, Corrosion behavior of nickel base alloys, stainless steel and titanium alloy in supercritical water containing chloride, phosphate and oxygen, Chem. Eng. Res. Des. 100 (2015) 530–541.
[41] J.R. Davis, ASM Specialty Handbook: Nickel, Cobalt, and Their Alloys, 2000.